

See discussions, stats, and author profiles for this publication at: <https://www.researchgate.net/publication/275895051>

The Stability of Amino-functionalized Polyhedral Oligomeric Silsesquioxanes (POSS) in Water

ARTICLE *in* THE JOURNAL OF PHYSICAL CHEMISTRY B · MAY 2015

Impact Factor: 3.3 · DOI: 10.1021/acs.jpcb.5b01955 · Source: PubMed

READS

25

7 AUTHORS, INCLUDING:



Monika Pilz

SINTEF

30 PUBLICATIONS 346 CITATIONS

[SEE PROFILE](#)



Nicolas Rival

SINTEF

7 PUBLICATIONS 31 CITATIONS

[SEE PROFILE](#)

The Stability of Amino-Functionalized Polyhedral Oligomeric Silsesquioxanes in Water

Sylvie Neyertz,^{*,†,‡} David Brown,^{†,‡} Monika Pilz,[§] Nicolas Rival,[§] Bjørnar Arstad,[§] Ferdinand Männle,[§] and Christian Simon[§]

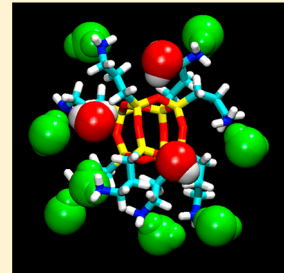
[†]LEPMI, Université Savoie Mont Blanc, F-73000 Chambéry, France

[‡]LEPMI, CNRS, F-38000 Grenoble, France

[§]SINTEF Materials and Chemistry, Forskningsveien 1, 0373 Oslo, Norway

Supporting Information

ABSTRACT: Octa(aminopropylsilsesquioxane) $\text{Si}_8\text{O}_{12}[(\text{CH}_2)_3\text{NH}_2]_8$ is a very important precursor for many other hybrid organic/inorganic polyhedral oligomeric silsesquioxanes (POSS) because of the reactivity of its primary amine groups. Unfortunately, it is unstable in water, which can lead to the cleavage of its siloxane cage. In the present work, such a degradation was confirmed using solid-state ^{29}Si NMR spectroscopy, and the molecular features at the basis of this instability were studied using molecular dynamics simulations (MD). It was also investigated whether replacing the primary amine end groups by secondary amines or by amides with long aliphatic chains could lead to an improvement in the water stability of the Si/O framework. In the pure bulk models, all POSS interdigitate with their pendant organic arms intertwined. Upon insertion of isolated molecules into water, the dimensions of the primary amine POSS remain close to those of the bulk, while the secondary amine and the amide POSS favor conformations that optimize the intramolecular chain–chain interactions. When there are several POSS molecules in water, they cluster with each other through both intra- and intermolecular chain–chain interactions. This tendency for the organic chains to intertwine whenever possible provides some protection to the siloxane cages from water, but also leaves some of the siloxane O exposed. As such, the latter are accessible to form transient hydrogen bonds with the water molecules, which could be a precursor step to hydrolysis and thus cage breakage. In the molecular models, a better protection was obtained in the amide POSS for two reasons: its chains tended to wrap efficiently around its cage, and its ketone O kept water from getting close to the siloxanes. The molecular modeling characterizations were found to agree very well with experimental evidence.



1. INTRODUCTION

Polyhedral oligomeric silsesquioxanes (POSS) with the chemical composition $(\text{RSiO}_{3/2})_8$ are hybrid organic–inorganic materials based on siloxane cages functionalized with a large variety of substituents R.^{1,2} Many different structures are possible depending on the nature of R, which are usually flexible organic chains with typical diameters of 1 to 3 nm. These POSS are commonly referred to as T_8R_8 since, in the nomenclature used for siloxane polymers, T denotes a silicon atom bonded to three oxygen atoms, in turn connected to other silicon atoms, and the fourth bond is with the pendant R group of the relatively rigid eight-corner Si_8O_{12} cage. Their versatility has led to several hundred different T_8R_8 compounds being prepared.^{1,3,4} They can be included as components in polymer blends to improve tensile properties, impact strengths, heat stabilities, gas barrier properties, and rheological properties.⁵

Octa(aminopropylsilsesquioxane) $\text{T}_8[(\text{CH}_2)_3\text{NH}_2]_8$ is a very important precursor for many T_8R_8 because of the reactivity of its primary amine end groups.² It can be synthesized using different approaches.¹ The most common route is through the acid-catalyzed hydrolytic condensation of $\text{Si}(\text{OEt})_3-(\text{CH}_2)_3\text{NH}_2$.⁶ This synthesis actually leads to the octahydrochloride salt, which is then converted to the free amine by

eluting methanolic or ethanolic solutions across an exchange resin. However, the neutralization to the free amine is difficult to obtain without compromising the Si/O framework, and in addition, $\text{T}_8[(\text{CH}_2)_3\text{NH}_2]_8$ decomposes rapidly when the solvent is removed.⁶ Alternatively, it can also be directly obtained from $\text{Si}(\text{OEt})_3(\text{CH}_2)_3\text{NH}_2$ when dissolved in various solvent mixtures with the basic Et_4NOH as a catalyst,^{7–9} or in mixtures of 1-propoxy-2-propanol and water associated with a heat treatment.⁵ Although the direct preparations of the free amine are supposed to lead to a more stable material than that obtained through the neutralization of the hydrochloride,¹ $\text{T}_8[(\text{CH}_2)_3\text{NH}_2]_8$ remains quite unstable in water, which can eventually lead to the cleavage of its Si/O framework. It has been postulated that it could be due to the water reacting with the free amine to form hydroxides and/or the amine nitrogen attacking silicon atoms, thus leading to an opening of the siloxane cage.⁶ Reactions using $\text{T}_8[(\text{CH}_2)_3\text{NH}_2]_8$ as a precursor or as a filler must thus be performed under conditions where framework degradation is avoided, and competing side

Received: February 27, 2015

Revised: May 4, 2015

Published: May 5, 2015

reactions do not occur. Another way of obtaining amino-based POSS is through nucleophilic substitution reactions on other POSS such as octakis(3-chloropropyl)octasilsesquioxanes.^{10,11} This allows for the siloxane cage to be efficiently functionalized with, for example, azide, phthalimide, or sulfobenzimidazole precursors, which can then be transformed into amines. However, the choice of the nitrogen nucleophile is very critical as it can also lead to cage rearrangements.^{10–12}

Solid-state ²⁹Si nuclear magnetic resonance (NMR) spectroscopy has become a widely used tool for the analysis of POSS compounds, as it can assess whether the siloxane cages have been degraded or not.^{1,13,14} An alternative would be to use mass spectroscopy, but MALDI-TOF spectra of POSS mixtures have been shown to be extremely complex.⁵ In the present work, we combine experimental characterizations using NMR for octa(aminopropylsilsesquioxane) along with fully atomistic classical molecular dynamics (MD) simulations¹⁵ to obtain insight into the molecular mechanisms leading to its degradation in water. To further investigate whether its stability in water can be improved by replacing the primary amines with secondary amines or with amides along with longer aliphatic chains, that is, in an attempt to better protect the inorganic cages, two other POSS structures were studied under the same conditions (Figure 1). The first system, which will be referred

adsorption layer around the cagelike silicate octamer $\text{Si}_8\text{O}_{20}^{8-}$ ⁴⁴ and expel the water in the vicinity of the siloxane oxygens. On the other hand, the hexamer $\text{Si}_6\text{O}_{15}^{6-}$ could not support such a layer, and as such, was more vulnerable to hydrolysis.⁴⁵ Other MD studies were aimed at describing POSS in the vicinity or within a membrane surrounded by water: $\text{Si}_8\text{O}_{12}\text{H}_8$ was found to partition near a water/lipid bilayer interface,⁴⁶ while $\text{Si}_8\text{O}_{12}(\text{OH})_8$ embedded within a polyamide membrane for seawater desalination increased its hydrophilicity.³⁴ Similarly, POSS slightly reduced the hydrophobic character of PP in PP/POSS nanocomposites.³³ Water can also be considered as a degradation product as colliding Kapton- $\text{Si}_8\text{O}_{12}\text{H}_6$ surfaces with high-energy atomic oxygen using a reactive force-field MD method led to separations of a few water molecules from the surfaces.³⁵ However, we are not aware of any MD simulations of pure POSS dissolved in water, and amino-functionalized POSS have only been simulated either in the pure state¹⁹ or in the presence of oxygen.⁴⁰

In this work, the experimental details and characterizations for the three POSS under study in water are first reported. This is followed by a brief description of the corresponding model preparations and MD simulation procedures, while more extensive details are provided in the Supporting Information. Afterward, we present the structural and dynamical analyses for the three model POSS and compare the modeling results to experimental evidence.

EXPERIMENTAL SECTION

Materials. Octa(aminopropylsilsesquioxane), that is, POSS-amine1, was synthesized at room temperature as described in ref 47. To synthesize POSS-amine2, POSS-amine1 (49% in 2-butoxyethanol; 7.56 g; 1 equiv) was dissolved in 75 mL of dimethylformamide. Na_2CO_3 (1.5 g; 14.54 mmol, 1 equiv) and 1-bromoocadecane (5.0 g; 14.54 mmol, 1 equiv) were added subsequently. The reaction was stirred at 373 K for 10 min, the white precipitate was filtered, washed twice with 20 mL of distilled water and once with 20 mL of ethanol, and dried under vacuum. To synthesize POSS-amide, POSS-amine1 (53% in 2-butoxyethanol; 34.50 g; 1 equiv) and stearic acid (38.2 g; 0.127 mol; 1 equiv) were dissolved in 290 g of xylene. The reaction was stirred at reflux for 3 h and was stopped when the expected amount of water was distilled off (~ 2.3 mL). It was then dried under vacuum.

The three structures were characterized using vibrational spectroscopy. The Fourier transform infrared (FTIR) spectra were recorded on a PerkinElmer Spectrum One FTIR spectrophotometer, and they are provided in the Supporting Information, along with the full identification of the main bands.^{1,48} All three spectra display a broad band at ca. 1120 cm^{-1} , which is characteristic of the Si—O—Si linkage in POSS cage compounds, and is usually considered as an indicator that the cage has not been cleaved during the synthesis process.¹ The POSS-amine1 spectrum also displays the characteristic bands of a primary aliphatic amine in the 1650–1580 and in the 900–650 cm^{-1} regions, the POSS-amine2 spectrum displays those of a secondary aliphatic amine in the 1580–1490 and 750–700 cm^{-1} regions, and the POSS-amide spectrum displays those of the amide group in the 1680–1630, 1570–1515, 1305–1200, and 770–620 cm^{-1} regions.

Note that these synthesis protocols were specifically developed for high-volume industrial applications with low-cost organic commodities and reasonable manufacturing costs.^{5,49–52} They involve the conversion of an amino-

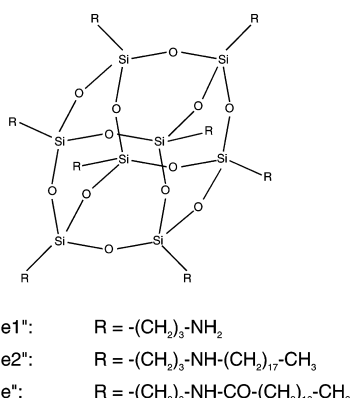


Figure 1. Chemical structures of the three POSS.

to hereafter as POSS-amine1, is the basic $\text{T}_8[(\text{CH}_2)_3\text{NH}_2]_8$ octa(aminopropylsilsesquioxane). The second system, POSS-amine2, is based on secondary amines with long aliphatic moieties, while in the third system, POSS-amide, the secondary amines were replaced by amides. The three chemical formulas are given in Figure 1.

Although this is essentially a simulation paper, comprehensive understanding of such systems by using both experimental evidence and molecular modeling is necessary to control and potentially use the different stabilities of POSS, and this information is an important element in designing T_8R_8 compounds with appropriate service lifetime in a product such as coatings. In the literature, most recent solid-state ²⁹Si NMR data for T_8R_8 compounds have been reviewed in ref 1. As far as MD simulations for T_8R_8 compounds are concerned, they include pure POSS,^{16–20} POSS with polymers, either as blends or as cross-linked systems,^{21–35} as well as POSS with small molecules.^{36–40} T_8R_8 as solutes have also been studied in melts of short poly(dimethylsiloxane) chains, hexadecane and hexane,^{23,41,42} or under a ligand form in dichloromethane.⁴³ In the specific cases of POSS-related/water interactions, tetraalkylammonium cations have been shown to form an

functionalized silane to an amino-functionalized POSS, followed by the development of organic branches using amine chemistry under fairly mild conditions, which limits degradation and/or cross-linking reactions of the amine-POSS during conversion.⁵ However, it is not possible to fully control the cage sizes and the substitution ratios: the syntheses do not only lead to T_8 -based POSS, but also to larger T_m with $m = 10\text{--}20$, while the number of R substituents can vary from 1 to 15–17, depending on the cage size.^{5,53,54} The final samples are thus mixtures of various cage sizes, although those based on $m = 8\text{--}12$ are the most common ones.⁵ Clearly, other synthesis protocols¹¹ could have improved the selectivity of the cage sizes and limited the number of byproducts. In addition, the use of a catalyst such as Na_2CO_3 may have led to extra cage rearrangements for POSS-amine2,¹² although its basicity is probably counteracted by the rapid production of HBr in the reaction. However, as noted above, our less-selective approach is aimed for industrial development, and as such, its disadvantages are compensated by the decrease of the manufacturing cost. Furthermore, as will be shown, all three systems can be discriminated by solid-state ^{29}Si NMR in spite of their complex composition.

Another point to emphasize is that although POSS-amine1 is soluble in many solvents, both POSS-amine2 and POSS-amide are only soluble in xylene and toluene at high temperatures. Within this context, purification with, for example, column chromatography, which has been reported for other nitrogen-based POSS compounds,^{10,11} would prove extremely difficult and probably not very efficient at isolating each structure.

To favor hydrolysis, 1 g of each sample was dissolved in a 40 mL water/40 mL xylene mixture, and stirred for several hours at 333 K. Two phases were always present, but the energetic stirring assured the contact between the POSS and water. The solvents were then distilled off, and the samples dried by freeze-drying.

Nuclear Magnetic Resonance Spectroscopy. As discussed elsewhere,^{1,13,14} ^{29}Si NMR was used to indicate whether the silica cages were intact or not after the hydrolysis treatment. As POSS-amine2 and POSS-amide are not soluble in common NMR solvents such as CDCl_3 ,¹ we could not use solution ^{29}Si NMR. Instead, such analyses were performed using solid-state ^{29}Si magic-angle spinning (MAS) NMR, even if its peaks are much broader and less well-defined than those obtained from solution NMR studies. For each sample, the experiment was performed at 11.7 T (500 MHz proton resonance frequency) using a Bruker Avance III spectrometer equipped with a 4.0 mm double resonance MAS probehead at room temperature at a MAS rate of 10 kHz. A single pulse transient experiment was performed using 2048 scans and a recycle delay of 20 s. The chemical shifts were referenced to TMS by the substitution method.⁵⁵ The solid-state ^{29}Si NMR spectra for all three POSS under study after the hydrolysis treatment are given in Figure 2.

The chemical shifts of the three amino-functionalized POSS are consistent with those recorded for a range of alkyl-substituted $T_8\text{R}_8$ compounds, which have also been shown to be in good agreement with solution ^{29}Si NMR studies.¹ As the organic chain linker $-(\text{CH}_2)_3-$ is identical in all structures, the three spectra show a major peak with chemical shifts around -67.5 ppm, which is attributed to intact siloxane cages. However, a shoulder to the main peak amounting to $\sim 30\%$ and another well-defined smaller peak at -59.7 ppm amounting to $\sim 15\%$ clearly appear in the POSS-amine1 spectrum (top curve of Figure 2). Both are assigned to reorganizations of the

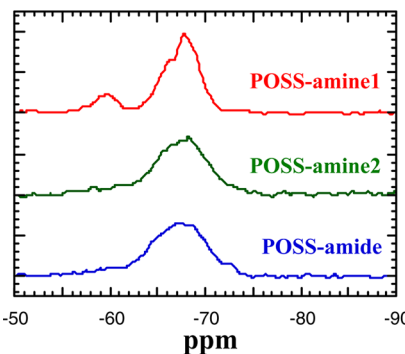


Figure 2. Solid-state ^{29}Si NMR spectra for POSS-amine1, POSS-amine2, and POSS-amide after hydrolysis.

siloxane cages due to Si–O linkage breaks in that sample. On the other hand, the POSS-amide spectrum (lower curve of Figure 2) does not exhibit such features, thus suggesting that its cages have remained largely intact. The POSS-amine2 spectrum (middle curve of Figure 2) appears to be an intermediate between the other two, with some small shoulders toward slightly higher chemical shifts on the major peak and some features at the same location than the smaller peak in POSS-amine1 (amounting to less than 10% of the total area). As noted before, these solid-state ^{29}Si NMR spectra were measured on complex $T_m\text{R}_n$ mixtures, and we are not aware of any data in the literature to unambiguously assign detailed chemical shifts to specific POSS degradation products.¹³ However, the general order that emerges with respect to water stability is clearly $\text{POSS-amine1} \ll \text{POSS-amine2} < \text{POSS-amide}$.

To better understand the basic molecular-level features behind these different stabilities with respect to water, the three POSS were studied using MD simulations. It was decided to restrict the models to the specific $T_8\text{R}_8$ form to eliminate the effects due to the different $T_m\text{R}_n$ compositions. As such, the direct effects of the organic chains on the water stability of the siloxane cages could be analyzed under exactly the same conditions for all three systems under study.

SIMULATION DETAILS

The classical MD simulations were performed using the gmq package,⁵⁶ either in its scalar or in its parallel form. Density functional theory calculations were performed with the Gaussian09 code⁵⁷ at the B3LYP/6-31G** level.

Using the same procedure as for other amino-functionalized POSS,^{19,40} the side chains and a $T_8\text{H}_8$ inorganic cage were first geometry-optimized separately with Gaussian09. For each system, the optimized chains were then attached to the cage, and the hybrid systems were reoptimized with Gaussian09. The average bond lengths and bond angles were extracted from the Gaussian09-minimized structures, while the partial charges were calculated using the Merz–Singh–Kollman procedure.^{58,59}

In the functional form of the classical force field used for the MD simulations,⁵⁶ the “bonded” interactions resulting from near-neighbor connections in the structures were described with angle-bending, torsional, and out-of-plane potentials. High-frequency modes, such as bond stretching or fast motions of the hydrogens in explicit CH_2 and CH_3 groups, were removed using rigid constraints with a relative tolerance of 1×10^{-6} .⁶⁰ It both allows for the use of a reasonable time step in the MD integration algorithm, that is, $\Delta t = 1 \times 10^{-15}$ s, and

Table 1. Characteristics of the Different Bulk and Solution Models under Study

systems	POSS-amine1 ^a		POSS-amine2 ^a		POSS-amide ^a	
			POSS bulks			
no. of POSS molecules		32		8		8
no. of atoms		3712		4384		4320
POSS concentration/g L ⁻¹	10 (1P)	50 (1P)	50 (8P)	50 (1P)	50 (8P)	50 (8P)
no. of POSS molecules	1	1	8	1	8	1
no. of water molecules	4900	950	7600	3050	24 400	3180
no. of atoms	14 816	2966	23 728	9698	77 584	10 080
no. of systems	3	3	3	3	1	3

^aThe parentheses refer to the number of POSS molecules in a solution model. The number of independent systems that were simulated is given in the last row.

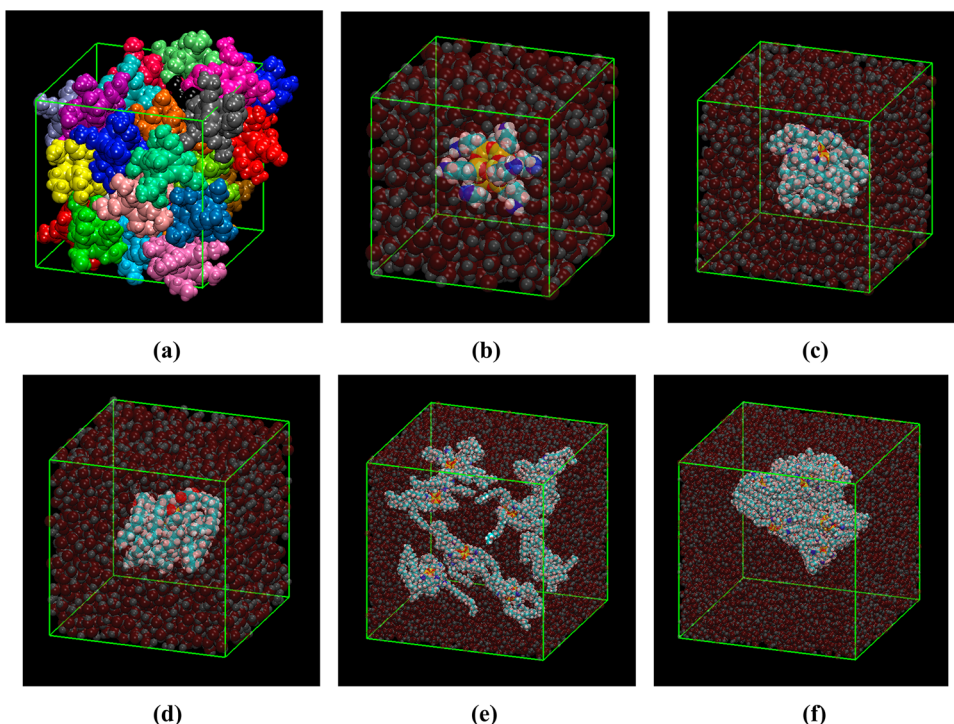


Figure 3. Schematic representations at the end of their respective production runs for (a) a pure bulk POSS-amine1 simulation with the different molecules being shown in different colors and (b–d) several POSS+water single-molecule 50 g L⁻¹ solution models. The water molecules are displayed using a transparent option of the VMD code. (b) A POSS-amine1. (c) A POSS-amine2. (d) A POSS-amide. (e, f) An 8-molecules POSS-amine2 system at the start and at the end of its production run, respectively. The volumes of the various simulation boxes are different and are given in Tables 2 and 3. The color code is the following: yellow = Si, red = O, cyan = C, blue = N, white = H.

avoids problems of equipartition of kinetic energy. The “nonbonded” excluded volume van der Waals and electrostatic potentials, which depend on the distance between two interacting sites, were applied to all atom pairs situated either on the same molecule (but separated by more than two bonds if the intervening angles are subject to the bending potential or by more than one bond otherwise) or on two different molecules. The long-range electrostatic potential was calculated using the Ewald summation method.^{61,62} The POSS force-field parameters were obtained either directly from the ab initio optimized structures or adapted from the literature.^{23,41,63–67} The water force-field parameters were taken from the extended single point-charge model, SPC/E,⁶⁸ which is known to provide a good representation of bulk water.^{69–71} All of them are given along with the atom types in the Supporting Information.

To prepare bulk POSS models, separate molecules were first decorrelated from their starting structures by sampling the gas-

phase configurations using the hybrid pivot Monte Carlo/molecular dynamics technique^{72–74} with all the intramolecular interactions switched on. Boxes containing 32 randomized molecules for POSS-amine1, and 8 for both POSS-amine2 and POSS-amide (Table 1), were densified and relaxed with MD for ~5000 ps at 700 K. They were then cooled to their target temperature of 333 K at a rate of -0.1 K ps^{-1} . Equilibration runs were performed until the densities stabilized, after which the pure bulk production runs continued up to 50000 ps, that is, 50 ns, at 333 K. In MD simulations of flexible molecules in hydrated systems, for example, proteins or polymers, it is notoriously difficult to obtain a satisfactory sampling of the different conformations at room temperature under the limited 1×10^{-15} to 1×10^{-9} s MD typical time scale.⁷⁵ The temperature of 333 K was thus chosen in order both to be experimentally realistic while being satisfactory in terms of effective conformational sampling. For similar reasons, Striolo

Table 2. Bulk Properties at 333 K

system	POSS-amine1 ^a	POSS-amine2 ^a	POSS-amide ^a
$\langle \rho_{\text{model}}^{333\text{K}} \rangle, \text{ g cm}^{-3}$	1.171 ± 0.001	0.831 ± 0.001	0.870 ± 0.001
$\langle V \rangle, \text{ nm}^3$	39.99 ± 0.03	46.37 ± 0.04	46.02 ± 0.05
$\langle U_{\text{pot}}^{\text{inter}} \rangle, \text{ kJ mol}^{-1}$	-283.4 ± 0.3	-731.9 ± 0.8	-755 ± 1
$\langle U_{\text{vdw}}^{\text{inter}} \rangle, \text{ kJ mol}^{-1}$	-238.3 ± 0.2	-727.4 ± 0.9	-730.6 ± 0.9
$\langle U_{\text{vdw cage-cage}}^{\text{inter}} \rangle, \text{ kJ mol}^{-1}$	-14.9 ± 0.1	-1.6 ± 0.1	-1.7 ± 0.1
$\langle U_{\text{vdw chain-chain}}^{\text{inter}} \rangle, \text{ kJ mol}^{-1}$	-118.9 ± 0.2	-640 ± 1	-643 ± 1
$\langle U_{\text{vdw cage-chain}}^{\text{inter}} \rangle, \text{ kJ mol}^{-1}$	-104.5 ± 0.2	-85.8 ± 0.9	-85.9 ± 0.9
$\langle U_{\text{coul}}^{\text{inter}} \rangle, \text{ kJ mol}^{-1}$	-45.1 ± 0.3	-4.5 ± 0.3	-24.6 ± 0.2
$\langle S^2 \rangle, \text{ \AA}^2$	31.81 ± 0.03	158.1 ± 0.2	164.6 ± 0.3
$\langle r_{\text{cage center-end}} \rangle, \text{ \AA}$	7.1 ± 0.1	17.0 ± 0.1	18.6 ± 0.1
$\langle r_{\text{Si-end}} \rangle, \text{ \AA}$	4.9 ± 0.1	16.1 ± 0.1	17.5 ± 0.1

^aResults are displayed with their associated standard errors. The kJ mol^{-1} are per POSS molecule.

et al. used a temperature range of 400–1000 K in their study of alkane-based POSS in hexadecane.⁴¹ All simulations were run under NpT conditions (constant number of atoms N , controlled isotropic pressure p , controlled temperature T). Most pure bulk simulation parameters were identical to those used before,^{19,40} and consequently only those that change, that is, $\alpha = 0.24$ and $K_{\max} = 9$ for an optimal convergence of the Ewald sums,⁷⁶ are reported here.

POSS+water solutions at 333 K were obtained by randomly selecting POSS molecules in the respective bulk models and inserting them^{73,75,77} into simulation boxes of pure SPC/E water at the typical experimental concentration of 50 g L⁻¹. A lower concentration of 10 g L⁻¹ was also attempted for POSS-amine1, but results were found to be similar to those at 50 g L⁻¹. Table 1 summarizes the different simulations that were run under NpT conditions for 35 ns, and shows that they amount to very large simulations boxes if the concentrations are to be kept in the experimental range. The simulations parameters for the solutions were identical to those of the bulk with the exception of the real-space cutoff for electrostatic interactions that was set to 13 Å, and the Ewald parameters that were set to $\alpha = 0.20$ for POSS-amine1, $\alpha = 0.17$ for POSS-amine2 and POSS-amide, and $K_{\max} = 12$ for all solutions. At the start, the POSS molecules were well-separated from each other even if, as will be shown later, the 8-molecules systems were generally found to cluster during the MD simulations.

Configurations were stored every 20 ps, and thermodynamical properties were stored every 1 ps for postanalyses. Schematic representations of several of these systems are displayed in Figure 3 using the VMD 1.8.2 visualization software.⁷⁸

THE POLYHEDRAL OLIGOMERIC SILSESQUIOXANES MODELS IN THE BULK AND IN AQUEOUS SOLUTIONS

In this section, the detailed analyses for the POSS models at the molecular level are reported both in their pure state and in their aqueous solutions. The latter are then used to complement the solid-state ²⁹Si NMR characterizations.

Bulk Properties. The bulk properties at 333 K were obtained from the MD pure bulk production runs averaged over their last 30 ns. Table 2 displays the average values for the model densities ρ , volumes V of the MD cells, and intermolecular potential energies U . It also reports several structural properties such as the POSS molecules mean-square radii of gyration $\langle S^2 \rangle$, the average distance between the center of a siloxane cage and its eight heavy end atoms (amine N for

POSS-amine1 and methyl C for both POSS-amine2 and POSS-amide) $\langle r_{\text{cage center-end}} \rangle$, along with the average distance between a Si and its organic arm heavy end-atom $\langle r_{\text{Si-end}} \rangle$. $\langle r_{\text{cage center-end}} \rangle$ can be associated with the overall dimensions of POSS molecules, while $\langle r_{\text{Si-end}} \rangle$ is more representative of their organic arm lengths.

As expected (Figure 1), the dimensions of POSS-amine1 are much smaller than those of POSS-amine2 and POSS-amide. As such, in POSS-amine1, there are more Si/O cages per unit volume, and thus its mass density $\langle \rho_{\text{model}}^{333\text{K}} \rangle$ is the highest. As for other amino-functionalized POSS,¹⁹ the cohesive energies $\langle U_{\text{pot}}^{\text{inter}} \rangle$ are dominated by the van der Waals (vdw) components $\langle U_{\text{vdw}}^{\text{inter}} \rangle$, and especially by their chain–chain contribution (Table 2). This is consistent with the POSS molecules having their pendant organic arms intertwined. The inorganic siloxane cage–cage contributions remain small, which suggests that the T₈ cages are dispersed in the bulks, while the cage–chain contributions originate mostly from pendant chains coming close to other cages through chain–chain interdigititation. It is not possible to resolve the more limited Coulombic component $\langle U_{\text{coul}}^{\text{inter}} \rangle$ in the same way as the vdw because of the chain and cage fragments not being individually electrically neutral in the Ewald sum. However, the electrostatic contributions reported in Table 2 do suggest the formation of hydrogen bonds in both POSS-amine1 and POSS-amide.

Intramolecular and intermolecular radial distribution functions $g(r)$ (for typical examples, see, e.g., ref 19) confirm that the siloxane cages are dispersed in the bulk models, while cage–ring and ring–ring separations are consistent with the POSS molecules having their pendant arms intertwined (Figure 3a). Close interactions are governed by very local factors, but there is a preference for intermolecular interactions because of steric considerations. As explained above, POSS-amine1 has closer POSS–POSS interactions than the other two systems. However, the indiscriminate intermolecular $g(r)$ do not show sharp peaks associated with long-range crystalline order. It has been reported experimentally that POSS-amine1 is able to crystallize during its synthesis, but this only happens after 12 h, a time scale that is far too long to be probed by MD techniques. In addition, the experimental powder diffractograms issued from two different studies on the same material⁷⁹ look rather different, even if there is a peak in both cases at 2θ values of ~10°. Applying Bragg's law for diffraction leads to d -spacings of ~8–9 Å, which is in very good agreement with the POSS-amine1 $\langle r_{\text{cage center-end}} \rangle$ (considering that the hydrogens are omitted). Such peaks are found in many diffraction studies on T₈R₈ compounds, and their d -spacings have indeed been

attributed to the overall dimensions of the POSS molecules.¹ As far as POSS-amine2 and POSS-amide are concerned, we are not aware of any experimental crystal structures. Crystalline T₈R₈ structures reported in the literature^{1,11,79} are usually molecules with much shorter pendant chains. In addition, POSS with large flexible chains have been shown to be prone to disorder.^{80,81}

Radial distribution functions are also useful to identify specific interactions such as hydrogen bonds. H-bonds are usually defined using either simple geometrical criteria^{82,83} or from the position of the first minimum after the first peak in the $g(r)$ for the donor hydrogen and acceptor species, that is, ~2.9 Å here. Such an interaction is very clear in POSS-amide, with ~33% of the amide oxygens being H-bonded to other amide hydrogens. A H-bonding peak can also be identified in POSS-amine1, with ~42% of the primary amine nitrogen being H-bonded to other primary amine hydrogens. Such H-bonds, which improve the POSS–POSS cohesion,¹⁹ are correlated to more negative electrostatic energies and higher densities (Table 2). In the case of POSS-amine2, no H-bonding network could be identified as the secondary amine is a much weaker hydrogen donor/acceptor group than both the primary amine and amide.

Relaxation of Polyhedral Oligomeric Silsesquioxanes Molecules upon Insertion into Water. Upon insertion into water, the POSS molecules adjust to the aqueous environment over a period of ~15 ns, as can be clearly seen from the time evolution of their mean-square radii of gyration ($\langle S^2 \rangle$) (Figure 4).

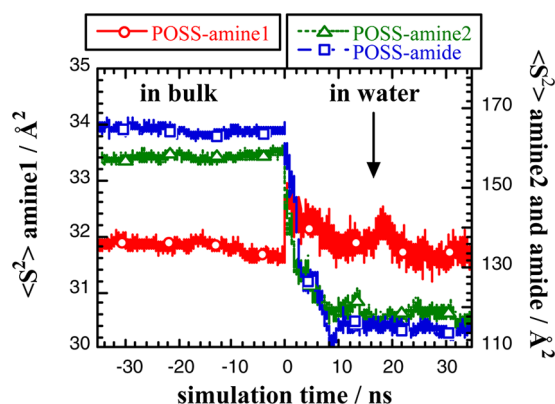


Figure 4. Time evolution of the mean-square radii of gyration ($\langle S^2 \rangle$) for some eight-molecule systems before and after being put in water. The time origin is set at the start of the POSS+water simulations. The POSS-amine2 and POSS-amide curves are displayed on a different scale (right axis) to correctly visualize the POSS-amine1 curve (left axis). Standard errors are on the order of 0.3 Å² for POSS-amine1 and of 7 Å² for POSS-amine2 and POSS-amide.

Consequently, this relaxation phase will be discarded from the subsequent analyses, and all results for the POSS+water simulations will be averaged over the last 20 ns of their ~35 ns production runs.

Aqueous Solution Properties. Some solution model properties at 333 K are reported in Table 3. The model densities of these dilute solutions, $\langle \rho_{\text{model}}^{333\text{K}} \rangle$, are all very close to the experimental density of liquid water at 333 K, 0.983 g cm⁻³.⁸⁴ The cohesive energies (not shown) are almost exclusively dominated by the water–water interactions and their strong capacity to create extended H-bond networks. The POSS–POSS interactions in the eight-POSS models amount to ~30–35% of their values in the pure bulks (Table 2), which suggests the formation of clusters (Figure 3e,f). This is confirmed by the relative POSS–water interactions being more negative for the single-molecule (1P) POSS than for the eight-POSS (8P) models. The tendency for POSS compounds to aggregate has already been described elsewhere both in experiment and in simulations,^{85–88} and specific organizations of neighboring POSS molecules have been shown to occur in nonaqueous solvents.^{41,42} As far as water is concerned, this clustering ability is reflected in some POSS-core dendrimers being able to form water-soluble networks encapsulating hydrophobic biological molecules.⁸⁹ The aggregation of POSS-amine1 has also been reported in the fabrication of POSS/carboxymethylcellulose hybrid hydrogels.⁹⁰ The structural parameters displayed in Table 3 will be analyzed hereafter.

Structures of POSS-Amine1 in Water. Figure 4 and Tables 2 and 3 show that the overall dimensions of POSS-amine1 in aqueous solution remain approximately the same as in the bulk. Figure 5 displays the probability density distributions for the organic arm lengths $r_{\text{Si-end}}$. Regardless of the dilution or of the presence of several POSS (Figure 5a), all distributions display the same three peaks, which are also found in the bulk. Integrating their areas gives ~11% for the first small peak, ~52% for the second peak, and ~37% for the third peak. Further analyses show that these peaks can all be attributed to specific conformations of the Si–C–C–C and C–C–C–N dihedral angles. In the convention used here, a dihedral angle τ varies from -180° to $+180^\circ$, with $-60^\circ < \tau < 60^\circ$ being considered as a trans (T) conformation. Similarly, the gauche[−] (G[−]) and gauche⁺ (G⁺) conformations are those angles situated either in the $-180^\circ \leq \tau \leq -60^\circ$ or in the $60^\circ \leq \tau \leq 180^\circ$ intervals, respectively. In the angle names, the first atom mentioned is the one that is closer to the siloxane cage. The O–Si–C–C and C–C–N–H angles, which have a threefold symmetry, are found to occupy all three states equivalently. However, the Si–C–C–C are found to be half in a trans and half in gauche states, while the C–C–C–N angles are

Table 3. Solution Model Properties at 333 K

system ^a	POSS-amine1			POSS-amine2		POSS-amide	
POSS concentration, g L ⁻¹	10 (1P)	50 (1P)	50 (8P)	50 (1P)	50 (8P)	50 (1P)	50 (8P)
$\langle \rho_{\text{model}}^{333\text{K}} \rangle$, g cm ⁻³	0.978	0.987	0.987	0.969	0.968	0.971	0.970
$\langle V \rangle$, nm ³	151.4	30.3	242.3	99.1	793.6	103.1	825.5
$\langle S^2 \rangle$, Å ²	32.2	31.6	31.8	105	123	82.1	118
$\langle r_{\text{cage center-end}} \rangle$, Å	7.2	7.1	7.1	13.0	16.0	13.4	14.6
$\langle r_{\text{Si-end}} \rangle$, Å	4.9	4.9	4.9	12.9	15.6	13.3	15.5

^aThe maximum standard errors are 0.002 g cm⁻³ on the densities, 0.1 nm³ on the volumes, 0.2 Å² on the POSS-amine1 $\langle S^2 \rangle$, 9 Å² on the POSS-amine2 and POSS-amide $\langle S^2 \rangle$, and 0.1 Å on the distances.

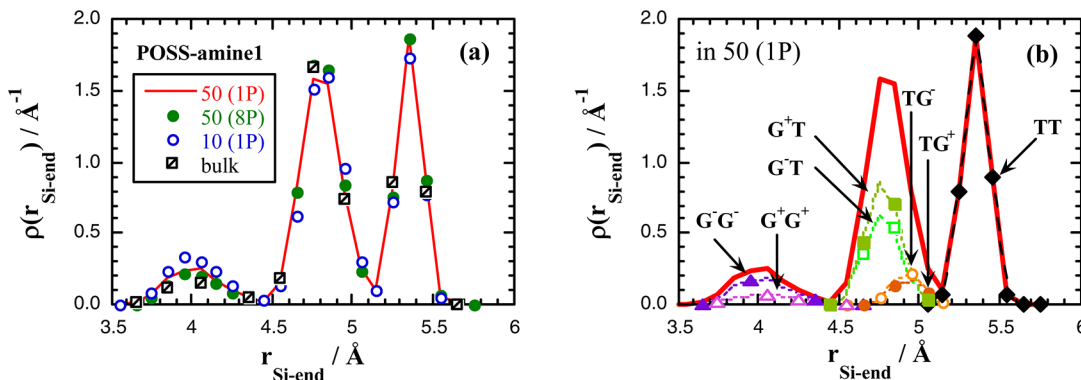


Figure 5. (a) Probability density distributions for the $r_{\text{Si-end}}$ distances in several POSS-amine1 systems. The number in the legend refers to the concentration in g L^{-1} with the number of POSS molecules given in brackets. The bulk distribution is also shown for comparison. (b) The contributions of the various Si–C–C–C/C–C–C–N conformer pairs to the probability density distribution for $r_{\text{Si-end}}$ in the 50 (1P) system. NB. These latter functions have not been symmetrized and the differences between TG^- and TG^+ , etc., are due to the limited statistics.

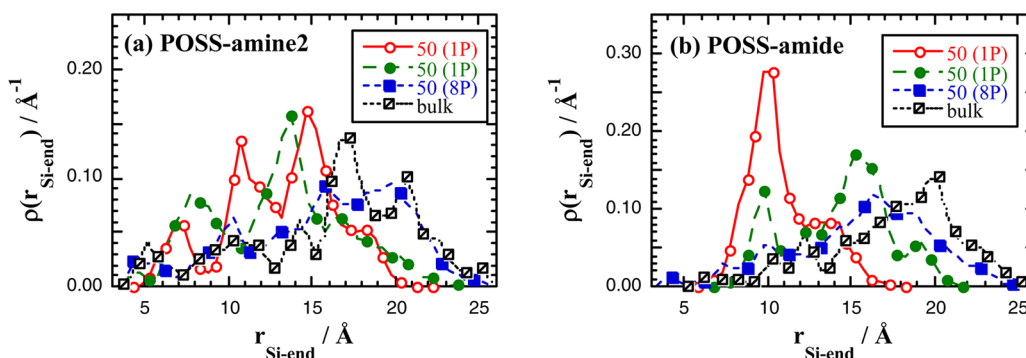


Figure 6. Probability density distributions for the $r_{\text{Si-end}}$ distances in (a) POSS-amine2 and (b) POSS-amide. The numbers in the legend refer to the POSS concentration in g L^{-1} with the number of POSS molecules given in brackets; the results for two different 1P simulations are shown for each system. The bulk distributions are also displayed for comparison.

predominantly in the trans state. Figure 5b displays a resolution of the distributions according to the sequence of states of those two torsions, which shows that the $r_{\text{Si-end}}$ distributions can indeed be directly correlated to the sequences of specific Si–C–C–C/C–C–C–N conformer pairs. The $\text{G}^- \text{G}^-$ and $\text{G}^+ \text{G}^+$ pairs make up the first peak. The $\text{G}^- \text{G}^+$ and $\text{G}^+ \text{G}^-$ conformers are relatively rare in comparison. The second peak is due to the sum of the $\text{G}^- \text{T}$, $\text{G}^+ \text{T}$ and TG^- , TG^+ conformers. The third peak is exclusively due to the TT conformers. Similar percentages were obtained for the bulks, although 4% of conformers were found in the $\text{G}^- \text{G}^+$ and $\text{G}^+ \text{G}^-$ states, which resulted in a few even lower $r_{\text{Si-end}}$ distances than those shown in Figure 5 (not displayed). However, these differences remain very minor, and all results suggest that POSS-amine1 in water keeps a very similar structure to that in the bulk. The structure of POSS-amine1 is thus exclusively governed by its intramolecular torsional barriers, and on average, there are systematically \sim three extended arms (TT conformers), \sim four arms of intermediate lengths (TG and GT conformers), and \sim one very coiled arm ($\text{G}^\pm \text{G}^\pm$ conformers) per molecule.

Structures of POSS-Amine2 and POSS-Amide in Water. Unlike POSS-amine1, Figure 4 and Tables 2 and 3 show that POSS-amine2 and POSS-amide conformations are different in water. Figure 6 displays their respective probability density distributions for the arm lengths $r_{\text{Si-end}}$. These distributions are the result of sequences of many more torsion angles, so they cannot be related to simple conformer pairs.

For POSS-amine2 in water (Figure 6a), some angles such as C–C–C–N and N–C–C–C have a strong bias toward the trans state (>80%); others such as C–C–C–C are found to be \sim 65% trans, while others such as Si–C–C–C, C–C–N–C, and C–N–C–C are \sim 50% trans and \sim 50% gauche. The bulk averages are rather close to those in solution, albeit with a few more angles being found in the trans state. Associated with the very flexible nature of the aliphatic chain, the successions of the various angles led to a wide variety of $r_{\text{Si-end}}$ distances. Indeed, the large number of combinations renders it difficult to obtain fully converged distribution functions. For example, those obtained from two independent single-molecule POSS-amine2 simulations are shown in Figure 6a (○ and ●), and they are clearly slightly different. However, their dimensions are always smaller than those in the eight-molecule POSS-amine2 in water system, whose curve almost superimposes with that of the bulk. This confirms that in water, the POSS try to cluster in a way analogous to the bulk, that is, through (mostly intermolecular) chain–chain interdigititation. Visualization of the configurations (Figure 3) shows that the pendant chains of isolated POSS molecules in water also try to cluster, but, for steric reasons, it is obviously a lot more difficult when the chains are attached to the same cage. The chains thus end up having conformations that permit the arms to come closer together, and this inevitably leads to smaller overall $r_{\text{Si-end}}$ dimensions.

The structures of POSS-amide in water (Figure 6b) resemble those of POSS-amine2, thus confirming that they are mostly governed by the flexibility of the aliphatic chains. However, if

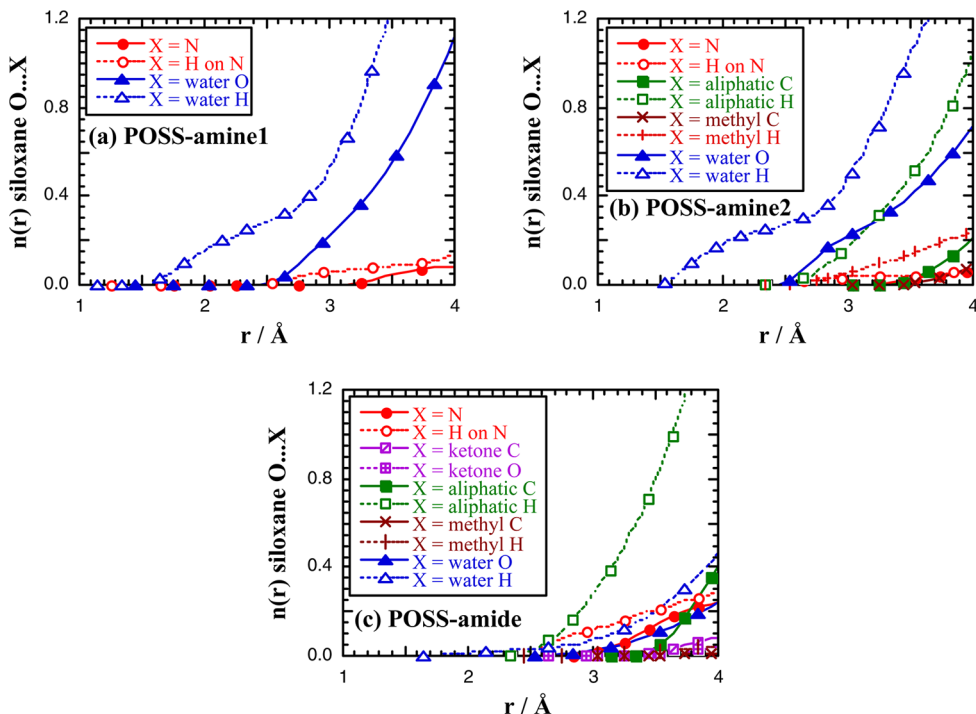


Figure 7. $n(r)$ functions for interactions between the siloxane cage O and several other atoms of type X in the three 50 g L^{-1} single-molecule POSS solutions. These functions give the average number of atoms of type X in a circle of radius r around a cage O atom.

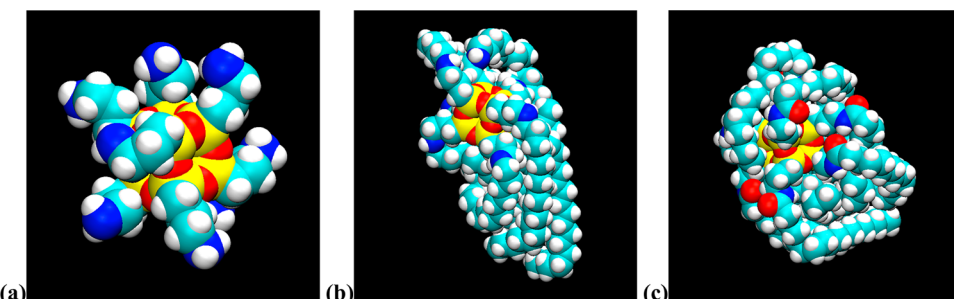


Figure 8. Space-filling snapshots of (a) POSS-amine1, (b) POSS-amine2, and (c) POSS-amide molecules at the end of their production runs in water. The color code is the same as that in Figure 3.

the conformer probabilities are about the same for the Si—C—C—C, C—C—N—C, and C—C—C—C angles as those in POSS-amine2, there are less trans conformers ($\sim 65\%$) for the C—C—C—N angles. In addition, the amide C—N—C—C is 100% trans, but its neighboring N—C—C—C and C—C—C—C angles favor the gauche states. These specific gauche angle conformations around the amide group make folding toward the cage even more favorable than for the secondary amine, thus allowing for easier intramolecular chain—chain digitation. As before, the eight-molecules POSS-amide system forms a cluster due to intermolecular chain—chain interactions, which resembles the bulk structure.

Preferential Interactions around the Polyhedral Oligomeric Silsesquioxanes Cages in Water. Radial distribution functions $g(r)$ were used to characterize the structure around the POSS siloxane cages. The $g(r)$ for a given atom type with either the cage Si or cage O were rather similar, although those for the less-accessible Si were offset with respect to those for O. In addition, the $g_{A...B}(r)$ between atom types A and B were integrated to give the average number of atoms of type B within a radius r of an atom A, $n_{A...B}(r)$. The

$n(r)$ functions for the 50 g L^{-1} single-POSS systems with the siloxane cage O being type A and other atoms being type X are displayed on the same short-distance scale in Figure 7a–c.

Figure 7 shows that the average number of N groups (circles) within the close vicinity of a cage O remains small for all three POSS under study. This undermines the hypothesis of the amine nitrogen attacking the cage in POSS-amine1.⁶ Similarly, the $n(r)$ with X being the spacer triethyl C (not shown) are found to superimpose for the three POSS. The interactions between the siloxane cage and the spacer are thus exclusively dominated by near-neighbor intramolecular factors. On the other hand, the fact that the long aliphatic chains tend to fold on themselves in solution (Figure 6) means that some aliphatic H and C (squares) are able to come very close to the siloxane cage in both POSS-amine2 and POSS-amide. These are not chain “U-turns” as the $n(r)$ with the methyl C and H (crosses) remain less than 1 at short distances, and, indeed, when visualized, as in Figure 8, the aliphatic chains fold in a way that optimizes chain—chain interactions to such an extent that the cage is forced to be somewhat excluded from the aliphatic mass.

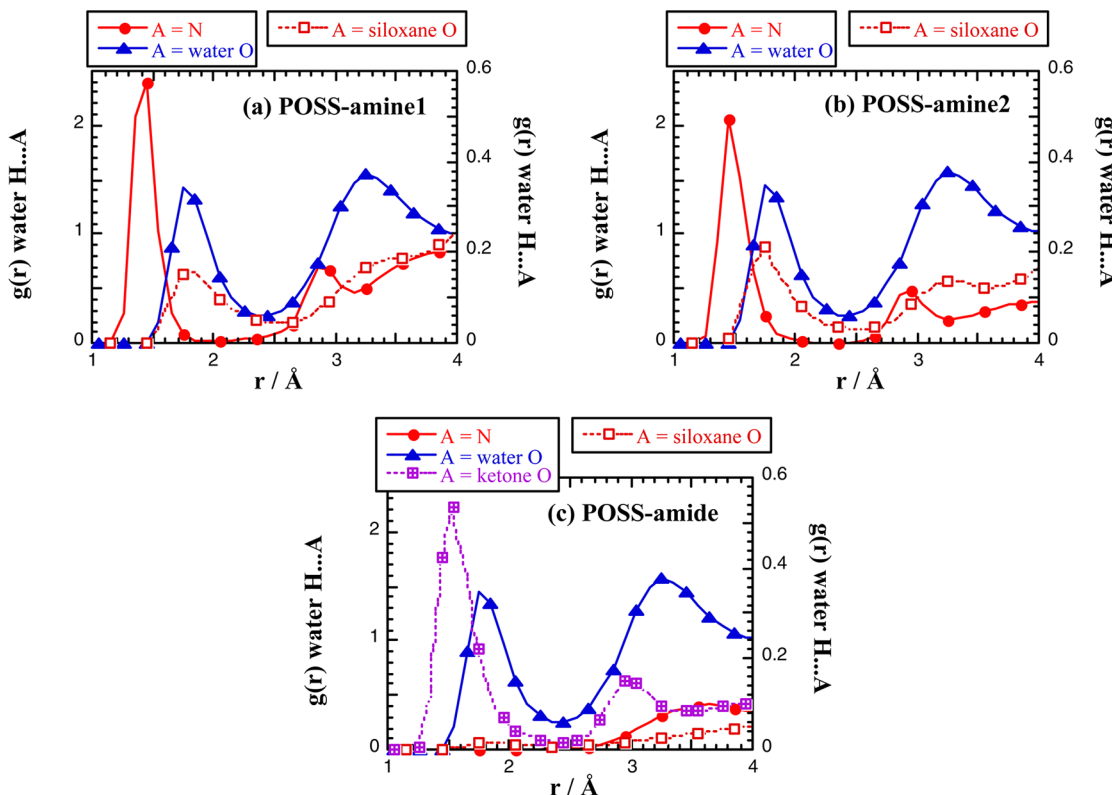


Figure 9. Average $g(r)$ functions for interactions between the water H and several acceptor A sites in the 50 g L^{-1} single-molecule POSS solutions. The axis on the left is for the hydrogen bonds formed with the N, the ketone O and the water O, while that on the right is for the less frequent hydrogen bonds formed with the siloxane O.

Water can only access the exposed parts of the cages, and Figure 7 shows that its closest interactions involve the water H (\triangle) rather than the water O (\blacktriangle). In POSS-amine1, access to the cage is only slightly restricted by the arms (Figure 8a), although their excluded-volume should not be underestimated. Interestingly, despite the competition with the aliphatic H, the POSS-amine2 siloxane O $n(r)$ with the water H is close to that in POSS-amine1 (Figure 7a,b), and this can be rationalized by observing that the POSS-amine2 chains fold while typically leaving one or two siloxane faces exposed to water (Figure 8b). Unlike POSS-amine1, at least one of these exposed siloxane faces in POSS-amine2 is always totally depleted as the chains attempt to interdigitate. The only system that displays a different behavior with respect to water is POSS-amide (Figure 7c), in which the chains are wrapped more efficiently around the cage because of its enhanced gauche conformations (Figure 8c). However, even there, part of the siloxane cage does remain exposed, and as such, the aliphatic arms are not sufficient to completely prevent water from getting close to the cage. There is obviously an important additional effect that originates from the specific interactions of water with the amide moiety. Indeed the ketone O (\blacksquare in Figure 7c) which, as will be seen later, are very favorable sites for H-bonding with water, are situated further away from the siloxane O than the amide N and tend to keep water from getting closer to the POSS-amide cage.

Hydrogen-Bond Structures. In the case of water, geometrical criteria to define H-bonds usually involve at least the distance between a water H and a hydrophilic acceptor site (A), but it can also use the value of the water O–H...A angle.^{34,82,83} Our experience^{75,91} is that this last criterion is not really discriminating, and so we just use the experimentally

quoted value of a water hydrogen bond being defined each time a water H is less than 2.4 \AA from a hydrophilic site.⁹² Indeed, Figure 9a–c, which displays the intermolecular $g(r)$ between a water H and potential hydrophilic sites shows that 2.4 \AA is the distance of the first minimum in the $g(r)$ for water H...water O. In addition, with this simple distance criterion, all angles involving H-bonds are above the angle criterion of 130° used elsewhere.^{82,83,93}

In POSS-amine1 (Figure 9a), the main hydrophilic sites for a water H are the primary amine N (\bullet) and the water O (\blacktriangle), while there is also a smaller peak with the siloxane O (\square). In POSS-amine2 (Figure 9b), the water form H-bonds with the same atoms, although the interaction with the secondary amine is a bit weaker than with the primary amine. In POSS-amide (Figure 9c), there are almost no H-bonds with the amide N, and they are replaced instead with a very strong hydrophilic interaction with the ketone O. The H-bonds with the POSS-amide siloxane cage are also much more attenuated. The intramolecular POSS–POSS H-bonds (not shown) were found to be negligible, that is, less than 4%, in the solutions of single POSS molecules. Almost all of them had been replaced by H-bonds with water instead.

Table 4 reports the average percentages of acceptors hydrogen-bonded with the water H when using the aforementioned distance criterion of 2.4 \AA .

While water is almost completely excluded from the POSS-amide cage, Table 4 confirms that $\sim 25\%$ of the siloxane O, that is, roughly three O of the 12 on the cage, form hydrogen bonds with water in both POSS-amine1 and POSS-amine2. Although this is expected for POSS-amine2, in which one or two siloxane faces are well exposed (Figure 8b), it seems more surprising for

Table 4. Average Percentages of Specific Acceptors Hydrogen-Bonded with the Water H in the 50 g L⁻¹ Single-Molecule POSS Solutions

acceptor	number of H-bonds	POSS-amine1 ^a	POSS-amine2 ^a	POSS-amide ^a
siloxane O	0	75.4	75.0	97.1
	1	24.3	24.6	2.9
	2	0.3	0.4	0.0
N	0	0.0	0.4	97.4
	1	93.4	99.2	2.6
	2	6.6	0.4	0.0
ketone O	0			0.3
	1			32.9
	2			61.8
	3			4.9
	4			0.1
water O	0	0.6	0.6	0.4
	1	28.6	28.5	27.0
	2	61.6	61.7	65.0
	3	9.0	9.0	7.5
	4	0.2	0.2	0.1

^aThe standard errors are less than 0.1%.

POSS-amine1, which lacks the protection of the long aliphatic chains, but in which all faces appear equally accessible (Figure 8a). However, as noted before, an average of five primary amine chains of eight are more or less folded (Figure 5), and as such, a large part of the cage is excluded to water. Figure 10a displays the probability density distributions for the distances between the amine N carried by near-neighbor organic branches in POSS-amine1, that is, those whose Si share a common cage O. These distances range from 3 to 14 Å, which clearly leaves some of the cage O depleted when their two branches on either side are far away from each other. However, from the present study, it is difficult to conclude whether the fact that POSS-amine1 and POSS-amine2 have the same average number of siloxane O H-bonded with water is a general feature of these systems, as this would require a systematic study of more structures.

As far as the chain acceptors are concerned, both amine N are systematically H-bonded with water, with the primary amine being marginally a better acceptor for double H-bonds than the secondary amine. On the other hand, the amide N can only form very few H-bonds, as it is close to a much stronger acceptor, the ketone O. Indeed, the ketone O is mostly found H-bonded with two water H, and it can even accept up to four

H-bonds at the same time. In the case of the water H···water O interactions, the percentages are rather similar in all three system under study as they are dominated by the dilutions and the capacity of water to form H-bonds in pure water. The fact that most model water molecules are H-bonded to two hydrophilic sites is in agreement with experiment.⁹⁴

In terms of geometry, the water O–H···A angle (Figure 10b) distributions are all found to be Gaussian and predominantly centered at 180°, regardless of the POSS under study. Second-order Legendre polynomial functions $P_2(\cos\theta)$ analyses⁷³ (not displayed) show that at short distances, the water molecules tend to place themselves more perpendicular than parallel with respect to the faces of the cages. In addition, there are less than an average of 0.3 water molecules linking two H-bonding sites on the POSS molecules, so POSS-water-POSS bridges⁷⁵ are almost nonexistent.

The overall picture that emerges is summarized in Figure 11, which shows snapshots of the three POSS under study along with the different water molecules that are H-bonded to them at the time of the snapshot. Please note that, in the color version, the water molecules H-bonded to the cage O are displayed in red and white, those H-bonded to N are displayed in green, and those H-bonded to the ketone O are displayed in mauve to better differentiate them.

Figure 11 confirms that, in spite of their primary and secondary amines being all H-bonded to water, part of the siloxane cage remains accessible to water in POSS-amine1 and POSS-amine2. On the other hand, POSS-amide is better protected, both because of its more efficient folding and because of the very strong ketone O-acceptor. In this system, it is much more difficult for water to access its siloxane cage.

Hydrogen-Bond Dynamics. The dynamics of the H-bonds were analyzed in two standard ways.⁷⁵ First, continuous lifetimes τ_c of individual H-bonds were obtained^{82,93} from simulations of 10 ps with the configurations being stored at every 1 fs time step. The τ_c are characteristic of the very short-time behavior and are reported in Table 5.

The high resolution used here shows that the τ_c typically span a region between 0.1 and 0.7 ps. As found elsewhere,⁷⁵ 1 ps would be a long continuous lifetime whatever the type of H-bond. The shortest-lived H-bonds are those with the primary amine and amide N. For the secondary amine N, the H-bonds seem on average more stable in spite of the large standard error. Indeed, the secondary amines are less accessible because of the aliphatic chains (Figure 11b), and there is probably less

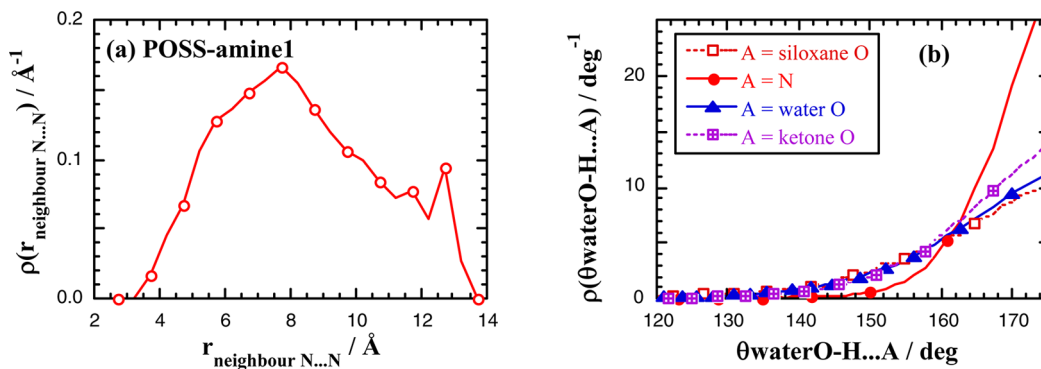


Figure 10. Probability density distributions for (a) the $r_{\text{neighbor N...N}}$ distances between the amine N carried by immediate near-neighbor chains in POSS-amine1 and (b) the water O–H···A angles in POSS-amine1 (for A = siloxane O, N, and water O) along with the water O–H···ketone O angles (purple squares with plus symbols) from POSS-amide.

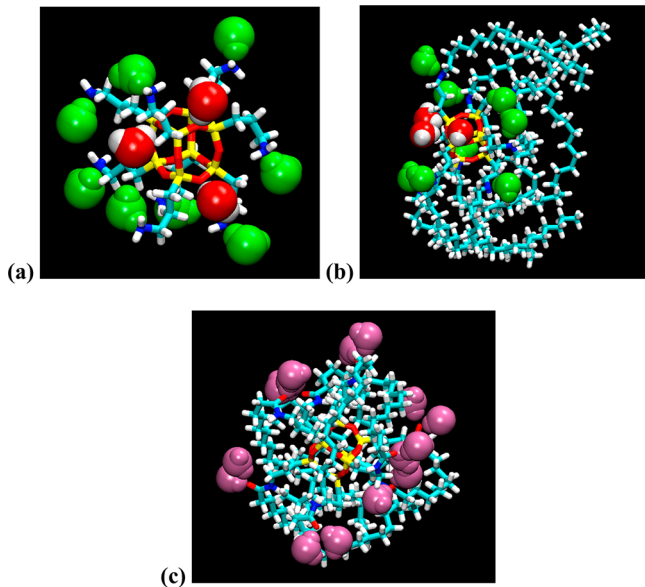


Figure 11. Snapshots of (a) POSS-amine1, (b) POSS-amine2, and (c) POSS-amide molecules along with their H-bonded waters. For clarity, the POSS are displayed in a bond representation, and their color code is the same as that in Figure 3. The water molecules are displayed in a space-filling representation, and their color depends on the acceptor: red and white for the siloxane O, green for the N, and mauve for the ketone O.

Table 5. Continuous Water O–H \cdots A H-Bond τ_c Lifetimes in Picoseconds as a Function of the Acceptor

H-bond acceptor	POSS-amine1 ^a	POSS-amine2 ^a	POSS-amide ^a
siloxane O	0.31 ± 0.06	0.33 ± 0.07	0.3 ± 0.1
N	0.14 ± 0.07	0.7 ± 0.5	0.08 ± 0.02
ketone O			0.6 ± 0.1
water O	0.341 ± 0.003	0.339 ± 0.002	0.340 ± 0.002

^aThe average values are given with their standard error.

competition between the N either with the other N or with the siloxane O than in POSS-amine1 (especially when the short chains are folded). An additional simulation of a pure 2016-molecule bulk water model was performed for comparison, and the continuous water O–H \cdots water O H-bond lifetimes were found to be 0.338 ± 0.002 at 333 K, that is, very similar to the water–water H-bonds in the diluted POSS solutions. Continuous H-bonds with the siloxane O are of the same order of magnitude than the standard H-bonds in water, while those with the strong amide ketone O acceptor are more stable.

A well-known problem with the aforementioned continuous lifetime analysis is that it does not give any information about the reformation of the same H-bond. It has been shown that this shortcoming can be circumvented using a correlation function analysis,^{95,96} which gives the probability of an H-bond still existing between two specific atoms at some later time, given that it did exist at the time origin.^{75,91} As it could have been broken and reformed several times in the intervening time, it does not give the same information as the continuous lifetime analysis. These relaxation functions all showed a similar behavior, which could be fitted to a stretched exponential Kohlrausch–Williams–Watts form.⁸² The area under the curves gives the average correlation times τ , which are characteristic of a longer-time behavior than τ_c and are reported in Table 6.

Table 6. Water O–H \cdots A H-Bond Correlation Times τ in Picoseconds as a Function of the Acceptor^a

H-bond acceptor	POSS-amine1	POSS-amine2	POSS-amide
siloxane O	4.28 ± 0.03	10.98 ± 0.06	2.7 ± 0.1
N	72.8 ± 0.7	976 ± 14	0.37 ± 0.01
ketone O			19.6 ± 0.4
water O	2.28 ± 0.02	2.22 ± 0.02	2.21 ± 0.02

^aThe average values are given with their standard error.

The values of τ are typical of those found elsewhere^{75,82,91,97} and are indeed quite a bit longer than the τ_c . As expected though, their 1×10^{-9} to 1×10^{-12} s time scale reflects the high mobility of H-bond networks in water at 333 K. Interestingly, the correlation times for the siloxane O and the amine N are longer in POSS-amine2 than in POSS-amine1 in spite of their same average numbers (Table 4). This suggests once again that, in the vicinity of POSS-amine1, there are more frequent exchanges of water molecules, due to the lower steric hindrance of the side chains. In addition, water in POSS-amine2 tends to H-bond with completely depleted cage faces, which is likely to be rather stable. In the case of the ketone O, its τ are intermediate, which can be linked to its fairly good accessibility and its strength as an acceptor, along with its ability to form several H-bonds at the same time.

In all cases, the hydrogen-bond network is very mobile. Over these 20 ns production simulations at 333 K, there are, for example, ~ 900 water molecules that have formed at some point an H-bond with a POSS-amine1 siloxane O, while ~ 2800 have formed an H-bond with a POSS-amide ketone O. Lowering the temperature will clearly slow such dynamics, but the mobility of water at room temperature still ensures that the main characteristics of this study should be conserved.

DISCUSSION: MODELING VERSUS EXPERIMENTAL EVIDENCE

The starting point of this study was to characterize the features at the basis of the instability in water of octa(aminopropylsilsesquioxane), that is, POSS-amine1. POSS-amine2 and POSS-amide were introduced to assess whether the stability in water could be improved by secondary amines or by amides along with longer organic chains. Solid-state ^{29}Si NMR was used to assess whether the POSS siloxane cages were intact or not after being in contact with water for several hours. In parallel, a series of MD simulations of T_8R_8 molecular models for each type of POSS in water were performed at experimental concentrations. The analyses around the model cages showed that its O is more accessible to the water H than its Si, thus suggesting that the siloxane O is the weakest point for the inorganic framework degradation.

In POSS-amine1, part of the available space around the cage is protected by some chains being folded close to it, but part of the near-neighbor branches are also further away from each other, thus leaving some of the siloxane O depleted. Such short organic chains are thus not capable of efficiently protecting the inorganic cage. This structural accessibility is associated in dynamical terms with very frequent exchanges of water molecules in the vicinity of the cage. This agrees with the enhanced susceptibility of POSS-amine1 to hydrolysis and its partial cage degradation as confirmed by its ^{29}Si NMR spectrum (top curve of Figure 2).

It had initially been thought that adding longer aliphatic chains such as in POSS-amine2 and POSS-amide would better

protect the siloxane cages. Indeed, in POSS-amide, the situation is significantly improved for two reasons: first, its chains wrap efficiently around its cage, thus exposing it less to water, and second, the ketone O, which are favorable sites for H-bonding, are very efficient at keeping water from getting close to the POSS-amide cage. Very few water molecules are able to come within the vicinity of its siloxane O, and as such, its cages are a lot less susceptible to hydrolysis. This is once again fully consistent with its ^{29}Si NMR spectrum, which shows no signs of cage degradation (lower curve of Figure 2).

On the other hand, the eight POSS-amine2 model chains aggregate in solution so much that they do not shield the entire cage from water, and leave some siloxane faces totally depleted. Consequently, the POSS-amine2 model is found to be as accessible to water as POSS-amine1, albeit for different reasons. Although the POSS-amine2 ^{29}Si NMR spectrum (middle curve of Figure 2) does not show the same clearly defined peak at -59.7 ppm than POSS-amine1, it does have some features in the same region (that are difficult to distinguish as they appear as a shoulder, $\sim 10\%$ of the total area, to the main peak). Similarly, there are also other small shoulders on the main peak. The POSS-amine2 ^{29}Si NMR spectrum can thus be considered as an intermediate between the other two POSS, even if it does not show the same degree of similarity as the models for POSS-amine1 and POSS-amine2 would suggest. There are several factors that could explain this. In the models, the main difference is the lower rate of water molecule exchanges in the vicinity of the secondary amine cage. This could make it harder to degrade than the primary amine cage. Another possibility is that the hydrolysis reaction was not performed for long enough (a few hours rather than a few days) to see more degradation in the experimental POSS-amine2 sample. However, a factor that is probably more critical is that the experimental sample is a complex mixture of T_mR_n ($m = 10-20$, $n = 1-17$) molecules, while the models are solely based on the T_8R_8 form. The long aliphatic chains will probably find it more difficult to aggregate with each other if the cage is larger and/or they are not branched to every Si of the cage. This may produce more coiled structures, thus protecting the cages better than in the symmetrical T_8R_8 form. To test this hypothesis would require many more models with different cage sizes and different linking points for the chains, as well as several starting structures for each specific T_mR_n needed for the simulation to have meaningful statistics. Although this is envisaged at a later point, it is beyond the limited scope of the present work.

As a whole though, the comparison between experimental evidence and molecular modeling is rather satisfactory, considering that such models remain simplified T_8R_8 versions of a much more complex reality. POSS-amine1 is clearly the most susceptible compound to hydrolysis, while a significantly better protection is obtained in POSS-amide. POSS-amine2 is an intermediate case in both modeling and experimental terms.

CONCLUSIONS

A combined experimental and molecular modeling study of three amino-functionalized POSS was performed to assess their different stabilities in water. The synthesis protocol led to complex T_mR_n mixtures with various siloxane cage sizes and organic chain attachment ratios. Solid-state ^{29}Si NMR data showed that such samples of both POSS-amine1 and POSS-amine2 were unstable in water, while POSS-amide was more stable.

To complement experimental evidence, a total of 20 different MD simulations were performed for the three POSS under study. The molecular models were restricted to the T_8R_8 form to eliminate the effects due to the different T_mR_n compositions. They clearly exhibited a transition in the water exposure of the inorganic cage going from POSS-amine1 (most exposed) to POSS-amide (least exposed). In addition, they showed that long aliphatic chains are not sufficient to better protect the inorganic cage. The organic chains need to be coiled around the cage and strong H-bond acceptors away from the cage are also definitely an asset.

Providing that the hydrolysis by water is the dominating mechanism underlying the siloxane cage breakage in these systems, both modeling and experimental data were thus in very good agreement about stability issues.

ASSOCIATED CONTENT

Supporting Information

FTIR characterization of the three POSS, description of molecular modelling, tabulated force field parameters data. The Supporting Information is available free of charge on the ACS Publications website at DOI: 10.1021/acs.jpcb.5b01955.

AUTHOR INFORMATION

Corresponding Author

*E-mail: sylvie.neyertz@univ-smb.fr. Phone: +33 4 79758697.

Notes

The authors declare no competing financial interest.

ACKNOWLEDGMENTS

This work was performed within the framework of the Centre of Excellence of Multifunctional Architectured Materials (CEMAM, No. AN-10-LABX-44-01). It was granted access to the HPC resources of CCRT/CINES/IDRIS under the allocations 2013-, 2014-, and 2015-095053 made by Grand Equipement National de Calcul Intensif (GENCI), France. The MUST cluster at the Univ. of Savoie (France) is also acknowledged for the provision of computer time.

REFERENCES

- (1) Cordes, D. B.; Lickiss, P. D.; Rataboul, F. Recent Developments in the Chemistry of Cubic Polyhedral Oligosilsesquioxanes. *Chem. Rev.* **2010**, *110*, 2081–2173.
- (2) *Applications of Polyhedral Oligomeric Silsesquioxanes*; Hartmann-Thompson, C., Ed.; Springer: Dordrecht Heidelberg London New York, 2011.
- (3) Reddy, B. S. R. *Advances in Nanocomposites - Synthesis, Characterization and Industrial Applications*; InTech Rijeka: Croatia, 2011.
- (4) Kuo, S.-W.; Chang, F.-C. POSS Related Polymer Nanocomposites. *Prog. Polym. Sci.* **2011**, *36*, 1649–1696.
- (5) Männle, F.; Tofteberg, T.; Skaugen, M.; Bu, H.; Peters, T.; Dietzel, P. D. C.; Pilz, M. Polymer Nanocomposite Coatings Based on Polyhedral Oligosilsesquioxanes: Route for Industrial Manufacturing and Barrier Properties. *J. Nanopart. Res.* **2011**, *13*, 4691–4701.
- (6) Feher, F. J.; Wyndham, K. D.; Soulivong, D.; Nguyen, F. Syntheses of Highly Functionalized Cube-Octameric Polyhedral Oligosilsesquioxanes ($R_8Si_8O_{12}$). *J. Chem. Soc., Dalton Trans.* **1999**, 1491–1497.
- (7) Zhang, Z.; Liang, G.; Lu, T. Synthesis and Characterization of Cage Octa(Aminopropylsilsesquioxane). *J. Appl. Polym. Sci.* **2007**, *103*, 2608–2614.
- (8) Zhang, Z.; Liang, G.; Ren, P.; Wang, J. Curing Behavior of Epoxy/POSS/DDS Hybrid Systems. *Polym. Compos.* **2008**, *29*, 77–83.

- (9) Seçkin, T.; Köytepe, S.; Adlgüzel, H. I. Molecular Design of POSS Core Star Polyimides as a Route to Low-K Dielectric Materials. *Mater. Chem. Phys.* **2008**, *112*, 1040–1046.
- (10) Ervithayasuporn, V.; Wang, X.; Kawakami, Y. Synthesis and Characterization of Highly Pure Azido-Functionalized Polyhedral Oligomeric Silsesquioxanes (POSS). *Chem. Commun.* **2009**, 5130–5132.
- (11) Jaroentomeechai, T.; Yingsukkamol, P.; Phurat, C.; Somsook, E.; Osotchan, T.; Ervithayasuporn, V. Synthesis and Reactivity of Nitrogen Nucleophiles-Induced Cage-Rearrangement Silsesquioxanes. *Inorg. Chem.* **2012**, *51*, 12266–12272.
- (12) Rikowski, E.; Marsmann, H. C. Cage-Rearrangement of Silsesquioxanes. *Polyhedron* **1997**, *16*, 3357–3361.
- (13) Huang, J.; He, C.; Liu, X.; Xu, J.; Tay, C. S. S.; Chow, S. Y. Organic–Inorganic Nanocomposites from Cubic Silsesquioxane Epoxides: Direct Characterization of Interphase, and Thermomechanical Properties. *Polymer* **2005**, *46*, 7018–7027.
- (14) Toepfer, O.; Neumann, D.; Roy-Choudhury, N.; Whittaker, A.; Matisons, J. Organic-Inorganic Poly(Methyl Methacrylate) Hybrids with Confined Polyhedral Oligosilsesquioxane Macromonomers. *Chem. Mater.* **2005**, *17*, 1027–1035.
- (15) Allen, M. P.; Tildesley, D. J. *Computer Simulation of Liquids*; Clarendon Press: Oxford, U.K., 1987.
- (16) Ionescu, T. C.; Qi, F.; McCabe, C.; Striolo, A.; Kieffer, J.; Cummings, P. T. Evaluation of Force Fields for Molecular Simulation of Polyhedral Oligomeric Silsesquioxanes. *J. Phys. Chem. B* **2006**, *110*, 2502–2510.
- (17) Capaldi, F. M.; Boyce, M. C.; Rutledge, G. C. The Mechanical Properties of Crystalline Cyclopentyl Polyhedral Oligomeric Silsesquioxane. *J. Chem. Phys.* **2006**, *124*, 214709.
- (18) Wann, D. A.; Zakharov, A. V.; Reilly, A. M.; McCaffrey, P. D.; Rankin, D. W. H. Experimental Equilibrium Structures: Application of Molecular Dynamics Simulations to Vibrational Corrections for Gas Electron Diffraction. *J. Phys. Chem. A* **2009**, *113*, 9511–9520.
- (19) Neyertz, S.; Brachet, P.; Brown, D.; Männle, F. The Structure of Amino-Functionalized Polyhedral Oligomeric Silsesquioxanes (POSS) Studied by Molecular Dynamics Simulations. *Comput. Mater. Sci.* **2012**, *62*, 258–265.
- (20) Abe, H.; Note, R.; Mizuseki, H.; Kawazoe, Y.; Habasaki, J.; Tomita, I. Thermal Behavior of Caged Silsesquioxane (POSS) Studied by Molecular Dynamics Simulations. *J. Inorg. Organomet. Polym.* **2012**, *22*, 845–851.
- (21) Bharadwaj, R. K.; Berry, R. J.; Farmer, B. L. Molecular Dynamics Simulation Study of Norbornene-POSS Polymers. *Polymer* **2000**, *41*, 7209–7221.
- (22) Capaldi, F. M.; Rutledge, G. C.; Boyce, M. C. Structure and Dynamics of Blends of Polyhedral Oligomeric Silsesquioxanes and Polyethylene by Atomistic Simulation. *Macromolecules* **2005**, *38*, 6700–6709.
- (23) Striolo, A.; McCabe, C.; Cummings, P. T. Thermodynamic and Transport Properties of Polyhedral Oligomeric Silsesquioxanes in Poly(Dimethylsiloxane). *J. Phys. Chem. B* **2005**, *109*, 14300–14307.
- (24) Patel, R. R.; Mohanraj, R.; Pittman, C. U., Jr. Properties of Polystyrene and Polymethyl Methacrylate Copolymers of Polyhedral Oligomeric Silsesquioxanes: A Molecular Dynamics Study. *J. Polym. Sci., Part B: Polym. Phys.* **2006**, *44*, 234–248.
- (25) Bizet, S.; Galy, J.; Gérard, J.-F. Molecular Dynamics Simulation of Organic-Inorganic Copolymers Based on Methacryl-POSS and Methyl Methacrylate. *Polymer* **2006**, *47*, 8219–8227.
- (26) Hao, N.; Böhning, M.; Goering, H.; Schönhals, A. Nanocomposites of Polyhedral Oligomeric Phenethylsilsesquioxanes and Poly(Bisphenol A Carbonate) as Investigated by Dielectric Spectroscopy. *Macromolecules* **2007**, *40*, 2955–2964.
- (27) Lacevic, N.; Gee, R. H.; Saab, A.; Maxwell, R. Computational Exploration of Polymer Nanocomposite Mechanical Property Modification Via Cross-Linking Topology. *J. Chem. Phys.* **2008**, *129*, 124903.
- (28) Lin, P.-H.; Khare, R. Molecular Simulation of Cross-Linked Epoxy and Epoxy-POSS Nanocomposite. *Macromolecules* **2009**, *42*, 4319–4327.
- (29) Zhang, Q. G.; Liu, Q. L.; Wu, J. Y.; Chen, Y.; Zhu, A. M. Structure-Related Diffusion in Poly(Methyl Methacrylate)/Polyhedral Oligomeric Silsesquioxanes Composites: A Molecular Dynamics Simulation Study. *J. Membr. Sci.* **2009**, *342*, 105–122.
- (30) Yani, Y.; Lamm, M. H. Molecular Dynamics Simulation of Mixed Matrix Nanocomposites Containing Polyimide and Polyhedral Oligomeric Silsesquioxane (POSS). *Polymer* **2009**, *50*, 1324–1332.
- (31) Song, X.; Sun, Y.; Wu, X.; Zeng, F. Molecular Dynamics Simulation of a Novel Kind of Polymer Composite Incorporated with Polyhedral Oligomeric Silsesquioxane (POSS). *Comput. Mater. Sci.* **2011**, *50*, 3282–3289.
- (32) Zeng, F.-L.; Sun, Y.; Zhou, Y.; Li, Q.-K. A Molecular Dynamics Simulation Study to Investigate the Elastic Properties of PVDF and POSS Nanocomposites. *Modell. Simul. Mater. Sci. Eng.* **2011**, *19*, 025005.
- (33) Smith, E. R.; Howlin, B. J.; Hamerton, I. Using POSS Reagents to Reduce Hydrophobic Character in Polypropylene Nanocomposites. *J. Mater. Chem. A* **2013**, *1*, 12971–12980.
- (34) Moon, J. H.; Katha, A. R.; Pandian, S.; Kolake, S. M.; Han, S. Polyamide-POSS Hybrid Membranes for Seawater Desalination: Effect of POSS Inclusion on Membrane Properties. *J. Membr. Sci.* **2014**, *461*, 89–95.
- (35) Rahnamoun, A.; van Duin, A. C. T. Reactive Molecular Dynamics Simulation on the Disintegration of Kapton, POSS Polyimide, Amorphous Silica and Teflon During Atomic Oxygen Impact Using the ReaxFF Reactive Force-Field Method. *J. Phys. Chem. A* **2014**, *118*, 2780–2787.
- (36) Haxton, K. J.; Cole-Hamilton, D. J.; Morris, R. E. The Structure of Phosphine-Functionalised Silsesquioxane-Based Dendrimers: A Molecular Dynamics Study. *Dalton Trans.* **2004**, 1665–1669.
- (37) Haxton, K. J.; Cole-Hamilton, D. J.; Morris, R. E. Silsesquioxane Dendrimers as Catalysts: A Bite-Sized Molecular Dynamics Study. *Dalton Trans.* **2007**, 3415–3420.
- (38) Wang, D.; Zhu, P.; Wei, S.; Hu, L. Influence of Molecular Structure of POSS on Gas-Molecule Diffusion Coefficients Using Molecular Dynamic Simulation. *Mater. Sci. Forum* **2011**, *689*, 114–121.
- (39) Roy, S.; Feng, J.; Scionti, V.; Jana, S. C.; Wesdemiotis, C. Self-Assembled Structure Formation from Interactions between Polyhedral Oligomeric Silsesquioxane and Sorbitol in Preparation of Polymer Compounds. *Polymer* **2012**, *53*, 1711–1724.
- (40) Neyertz, S.; Gopalan, P.; Brachet, P.; Kristiansen, A.; Männle, F.; Brown, D. Oxygen Transport in Amino-Functionalized Polyhedral Oligomeric Silsesquioxanes (POSS). *Soft Mater.* **2014**, *12*, 113–123.
- (41) Striolo, A.; McCabe, C.; Cummings, P. T. Effective Interactions between Polyhedral Oligomeric Silsesquioxanes Dissolved in Normal Hexadecane from Molecular Simulation. *Macromolecules* **2005**, *38*, 8950–8959.
- (42) Striolo, A.; McCabe, C.; Cummings, P. T.; Chan, E. R.; Glotzer, S. C. Aggregation of POSS Monomers in Liquid Hexane: A Molecular-Simulation Study. *J. Phys. Chem. B* **2007**, *111*, 12248–12256.
- (43) Ahmadi, A.; McBride, C.; Freire, J. J.; Kajetanowicz, A.; Czaban, J.; Grela, K. Force Field Parametrization and Molecular Dynamics Simulation of Flexible POSS-Linked (NHC; Phosphine) Ru Catalytic Complexes. *J. Phys. Chem. A* **2011**, *115*, 12017–12024.
- (44) Caratzoulas, S.; Vlachos, D. G.; Tsapatsis, M. Molecular Dynamics Studies on the Role of the Tetramethylammonium Cations in the Stability of the Silica Octamers $\text{Si}_8\text{O}_{20}^{8-}$ in Solution. *J. Phys. Chem. B* **2005**, *109*, 10429–10434.
- (45) Caratzoulas, S.; Vlachos, D. G.; Tsapatsis, M. On the Role of Tetramethylammonium Cation and Effects of Solvent Dynamics on the Stability of the Cage-Like Silicates $\text{Si}_6\text{O}_{15}^{6-}$ and $\text{Si}_8\text{O}_{20}^{8-}$ in Aqueous Solution. A Molecular Dynamics Study. *J. Am. Chem. Soc.* **2006**, *128*, 596–606.

- (46) Redmill, P. S.; McCabe, C. Molecular Dynamics Study of the Behavior of Selected Nanoscale Building Blocks in a Gel-Phase Lipid Bilayer. *J. Phys. Chem. B* **2010**, *114*, 9165–9172.
- (47) Helland, T.; Marstokk, O.; Männle, F.; Simon, C. R.; Juan, Y. Binder for Air-Drying Paint Comprising Nanoparticle Bonded Silicon Derivative of Unsaturated Fatty Acid, Wo 2009113876 A1, 2009.
- (48) Socrates, G. *Infrared Characteristic Group Frequencies*; John Wiley & Sons: Chichester, U.K., 1980.
- (49) Männle, F.; Simon, C. R.; Beylich, J.; Redford, K. Polybranched Organic/Inorganic Hybrid Polymer and Method for Its Manufacture, Wo2005100449, 2004.
- (50) Männle, F.; Simon, C. R.; Beylich, J.; Larsen, Å. G.; Hauge, R. P.; Kleppe, E. A.; Rodseth, K. R. Polymer Composition, Wo2005100469, 2004.
- (51) Männle, F.; Simon, C. R.; Beylich, J.; Sommer, B.; Hinrichsen, E. L.; Andreassen, E.; Olafsen, K.; Redford, K.; Didriksen, T. Method for the Manufacture of Polybranched Organic/Inorganic Hybrid Polymers, Wo2005100450, 2004.
- (52) Männle, F.; Rodseth, K. R.; Bu, H. Light Protective Additive Based on Organic/Inorganic Hybrid Polymer Method for Its Manufacture and Use Thereof, Wo2007053024, 2005.
- (53) Dell'Erba, I. E.; Fasce, D. P.; Williams, R. J. J.; Erra-Balsells, R.; Fukuyama, Y.; Nonami, H. Poly(Silsesquioxanes) Derived from the Hydrolytic Condensation of Organotrialkoxsilanes Containing Hydroxyl Groups. *J. Organomet. Chem.* **2003**, *686*, 42–51.
- (54) Zhang, X.; Huang, Y.; Wang, T.; Hu, L. Effects of Silsesquioxane Coating Structure on Mechanical Interfacial Properties of Carbon Fibre/Polyarylacetylene Composites. *J. Mater. Sci.* **2007**, *42*, 5264–5271.
- (55) Harris, R. K.; Becker, E. D.; Cabral de Menezes, S. M.; Goodfellow, R.; Granger, P. NMR Nomenclature: Nuclear Spin Properties and Conventions for Chemical Shifts. *Solid State Nucl. Magn. Reson.* **2002**, *22*, 458–483.
- (56) Brown, D. The Gmq User Manual Version 5. <http://www.lmops.univ-savoie.fr/brown/gmq.html> 2013.
- (57) Frisch, M. J.; Trucks, G. W.; Schlegel, H. B.; Scuseria, G. E.; Robb, M. A.; Cheeseman, J. R.; Scalmani, G.; Barone, V.; Mennucci, B.; Petersson, G. A. et al. *Gaussian 09*, Revision A.02; Gaussian, Inc.: Wallingford, CT, 2009.
- (58) Singh, U. C.; Kollman, P. A. An Approach to Computing Electrostatic Charges for Molecules. *J. Comput. Chem.* **1984**, *5*, 129–145.
- (59) Besler, B. H.; Merz, K. M., Jr.; Kollman, P. A. Atomic Charges Derived from Semiempirical Methods. *J. Comput. Chem.* **1990**, *11*, 431–439.
- (60) Hammonds, K. D.; Ryckaert, J.-P. On the Convergence of the Shake Algorithm. *Comput. Phys. Commun.* **1991**, *62*, 336–351.
- (61) Ewald, P. P. Die Berechnung Optischer Und Elektrostatischer Gitterpotentiale. *Ann. Phys.* **1921**, *369*, 253–287.
- (62) Smith, W. A Replicated Data Molecular Dynamics Strategy for the Parallel Ewald Sum. *Comput. Phys. Commun.* **1992**, *67*, 392–406.
- (63) Clark, M.; Cramer, R. D., III; Van Opdenbosch, N. Validation of the General Purpose Tripos 5.2 Force Field. *J. Comput. Chem.* **1989**, *10*, 982–1012.
- (64) Frischknecht, A. L.; Curro, J. G. Improved United Atom Force Field for Poly(Dimethylsiloxane). *Macromolecules* **2003**, *36*, 2122–2129.
- (65) Li, H.-C.; Lee, C.-Y.; McCabe, C.; Striolo, A.; Neurock, M. Ab Initio Analysis of the Structural Properties of Alkyl-Substituted Polyhedral Oligomeric Silsesquioxanes. *J. Phys. Chem. A* **2007**, *111*, 3577–3584.
- (66) Sok, R. M.; Berendsen, H. J. C.; Van Gunsteren, W. F. Molecular Dynamics Simulation of the Transport of Small Molecules across a Polymer Membrane. *J. Chem. Phys.* **1992**, *96*, 4699–4704.
- (67) Makrodimitri, Z. A.; Dohrn, R.; Economou, I. G. Atomistic Simulation of Poly(Dimethylsiloxane): Force Field Development, Structure, and Thermodynamic Properties of Polymer Melt and Solubility of N-Alkanes, N-Perfluoroalkanes, and Noble and Light Gases. *Macromolecules* **2007**, *40*, 1720–1729.
- (68) Berendsen, H. J. C.; Grigera, J. R.; Straatsma, T. P. The Missing Term in Effective Pair Potentials. *J. Phys. Chem.* **1987**, *91*, 6269–6271.
- (69) Heyes, D. M. Physical Properties of Liquid Water by Molecular Dynamics Simulations. *J. Chem. Soc., Faraday Trans.* **1994**, *90*, 3039–3049.
- (70) Guillot, B. A Reappraisal of What We Have Learnt During Three Decades of Computer Simulations on Water. *J. Mol. Liq.* **2002**, *101*, 219–260.
- (71) Zhang, Z.; Duan, Z. Prediction of the PVT Properties of Water over Wide Range of Temperatures and Pressures from Molecular Dynamics Simulation. *Phys. Earth Planet. Inter.* **2005**, *149*, 335–354.
- (72) Brown, D.; Clarke, J. H. R.; Okuda, M.; Yamazaki, T. A Molecular Dynamics Study of Chain Configurations in N-Alkane Liquids. *J. Chem. Phys.* **1994**, *100*, 1684–1692.
- (73) Neyertz, S. Tutorial: Molecular Dynamics Simulations of Microstructure and Transport Phenomena in Glassy Polymers. *Soft Mater.* **2007**, *4*, 15–83.
- (74) Neyertz, S. Gas Transport in Dense Polymeric Membranes, Molecular Dynamics Simulations. In *Encyclopedia of Membrane Science and Technology*; Hoek, E. M. V., Tarabara, V. V., Eds.; John Wiley & Sons: Hoboken, NJ, 2013.
- (75) Marque, G.; Neyertz, S.; Verdu, J.; Prunier, V.; Brown, D. A Molecular Dynamics Simulation Study of Water in Amorphous Kapton. *Macromolecules* **2008**, *41*, 3349–3362.
- (76) Fincham, D. Optimisation of the Ewald Sum for Large Systems. *Mol. Simul.* **1994**, *13*, 1–19.
- (77) Neyertz, S.; Brown, D.; Douanne, A.; Bas, C.; Albérola, N. D. The Molecular Structure and Dynamics of Short Oligomers of PMDA-ODA and BCDA-ODA Polyimides in the Absence and Presence of Water. *J. Phys. Chem. B* **2002**, *106*, 4617–4631.
- (78) Humphrey, W.; Dalke, A.; Schulten, K. VMD: Visual Molecular Dynamics. *J. Mol. Graphics* **1996**, *14*, 33–38.
- (79) Li, W.; Liu, F.; Wei, L.; Zhao, T. Allylated Novolac/4,4'-Bismaleimidodiphenylmethane Resin Containing Polyhedral Oligomeric Silsesquioxane: Preparation, Morphology and Thermal Stability. *J. Appl. Polym. Sci.* **2007**, *104*, 3903–3908.
- (80) Drylie, E. A.; Andrews, C. D.; Hearshaw, M. A.; Jimenez-Rodriguez, C.; Slawin, A.; Cole-Hamilton, D. J.; Morris, R. E. Synthesis and Crystal Structures of Bromo- and Ester-Functionalised Polyhedral Silsesquioxanes. *Polyhedron* **2006**, *25*, 853–858.
- (81) Bassindale, A. R.; Chen, H.; Liu, Z.; MacKinnon, I. A.; Parker, D. J.; Taylor, P. G.; Yang, Y.; Light, M. E.; Horton, P. N.; Hursthorne, M. B. A Higher Yielding Route to Octasilsesquioxane Cages Using Tetrabutylammonium Fluoride, Part 2: Further Synthetic Advances, Mechanistic Investigations and X-Ray Crystal Structure Studies into the Factors That Determine Cage Geometry in the Solid State. *J. Organomet. Chem.* **2004**, *689*, 3287–3300.
- (82) Müller-Plathe, F. Microscopic Dynamics in Water-Swollen Poly(Vinyl Alcohol). *J. Chem. Phys.* **1998**, *108*, 8252–8263.
- (83) Goudeau, S.; Charlot, M.; Vergelati, C.; Müller-Plathe, F. Atomistic Simulation of the Water Influence on the Local Structure of Polyamide 6,6. *Macromolecules* **2004**, *37*, 8072–8081.
- (84) Lide, D. R. *CRC Handbook of Chemistry and Physics*; 75th ed.; CRC Press Inc.: Boca Raton, FL, 1995.
- (85) Abad, M. J.; Barral, L.; Fasce, D. P.; Williams, R. J. J. Epoxy Networks Containing Large Mass Fractions of a Monofunctional Polyhedral Oligomeric Silsesquioxane (POSS). *Macromolecules* **2003**, *36*, 3128–3135.
- (86) Zhang, X.; Chan, E. R.; Glotzer, S. C. Self-Assembled Morphologies of Monotethered Polyhedral Oligomeric Silsesquioxanes Nanocubes from Computer Simulation. *J. Chem. Phys.* **2005**, *123*, 184718.
- (87) Chan, E. R.; Zhang, X.; Lee, C.-Y.; Neurock, M.; Glotzer, S. C. Simulations of Tetra-Tethered Organic/Inorganic Nanocube-Polymer Assemblies. *Macromolecules* **2005**, *38*, 6168–6180.
- (88) Li, Y.; Zhang, W.-B.; Hsieh, I.-F.; Zhang, G.; Cao, Y.; Li, X.; Wesdemiotis, C.; Lotz, B.; Xiong, H.; Cheng, S. Z. D. Breaking Symmetry toward Nonspherical Janus Particles Based on Polyhedral

- Oligomeric Silsesquioxanes: Molecular Design, "Click" Synthesis and Hierarchical Structure. *J. Am. Chem. Soc.* **2011**, *133*, 10712–10715.
- (89) Tanaka, K.; Chujo, Y. Unique Properties of Amphiphilic POSS and Their Applications. *Polym. J.* **2013**, *45*, 247–254.
- (90) Liu, H.; Huang, S.; Li, X.; Zhang, L.; Tan, Y.; Wei, C.; Lv, J. Facile Fabrication of Novel Polyhedral Oligomeric Silsesquioxane/Carboxymethyl Cellulose Hybrid Hydrogel Based on Supramolecular Interactions. *Mater. Lett.* **2013**, *90*, 142–144.
- (91) Marque, G.; Verdu, J.; Prunier, V.; Brown, D. A Molecular Dynamics Simulation Study of Three Polysulfones in Dry and Hydrated States. *J. Polym. Sci., Part B: Polym. Phys.* **2010**, *48*, 2312–2336.
- (92) Pimentel, G. C.; McClellan, A. L. *The Hydrogen Bond*; W. H. Freeman: San Francisco, CA, 1960.
- (93) Müller-Plathe, F.; Van Gunsteren, W. F. Solvation of Poly(Vinyl Alcohol) in Water, Ethanol and an Equimolar Water-Ethanol Mixture: Structure and Dynamics Studied by Molecular Dynamics Simulation. *Polymer* **1997**, *38*, 2259–2268.
- (94) Puffr, R.; Sebenda, J. On the Structure and Properties of Polyamides. XXVII. The Mechanism of Water Sorption in Polyamides. *J. Polym. Sci.: Part C* **1967**, *16*, 79–93.
- (95) Rapaport, D. C. Hydrogen Bonds in Water: Network Organization and Lifetimes. *Mol. Phys.* **1983**, *50*, 1151–1162.
- (96) Stillinger, F. H. Theory and Molecular Models for Water. *Adv. Chem. Phys.* **1975**, *31*, 1–101.
- (97) Borodin, O.; Bedrov, D.; Smith, G. D. Concentration Dependence of Water Dynamics in Poly(Ethylene Oxide)/Water Solutions from Molecular Dynamics Simulations. *J. Phys. Chem. B* **2002**, *106*, 5194–5199.